Three-component model and tricritical points: A renormalization-group study. II. General dimensions and the three-phase monohedron

Julia M. Yeomans and Michael E. Fisher
Baker Laboratory, Cornell University, Ithaca, New York 14853
(Received 24 March 1981)

In Part I the global phase diagram of the general spin-1, nearest-neighbor, ferromagnetic Ising model was studied for $d=2$ dimensions using an approximate renormalization-group approach of the Migdal-Kadanoff type. Here general d is considered with emphasis on $\epsilon=d-1$ expansions and on the variation of the tricritical exponents with $d\leq 4$. A dilution field is introduced which can be chosen to yield tricritical exponents for $d=2$, in better agreement with more reliable estimates and conjectured exact results. The three-phase monohedra, which describe the densities of coexisting phases near a tricritical point, are calculated quantitatively for $d=2$, and their shape contrasted with that predicted by classical theory: they are found, in particular, to be significantly flattened.

I. INTRODUCTION

An important task, still outstanding in the theory of multicritical phenomena, is to provide a detailed understanding of the equation of state of a system in the vicinity of a *tricritical point.* In particular, the interplay of the nonclassical critical and tricritical behavior in two- and three-dimensional systems and the precise role of the *four* relevant scaling fields requires further elucidation. Additionally, concrete numerical predictions describing three-phase coexistence near tricriticality in specific models are needed.

In the first part of this work[1] (to be denoted I) an attack on these problems was initiated using a real-space renormalization-group approach. Specifically a form of Migdal-Kadanoff approximate renormalization group[2] was used to study a spin-1 Ising model with Hamiltonian

$$-\frac{\mathcal{H}}{k_BT}=H\sum_i s_i-D\sum_i s_i^2+q^{-1}\sum_{\langle ij\rangle}[Js_is_j+Ks_i^2s_j^2+\tfrac{1}{2}H_3s_is_j(s_i+s_j)]\ . \tag{1.1}$$

Here the spin variables take the values $s_i=+1,0,-1$, while q is the coordination number of the lattice and the pair interactions act only between nearest neighbors. Note that the Hamiltonian (1.1) includes all single-site and nearest-neighbor pair interactions which respect the full symmetry of the lattice.

The fixed-point topology and corresponding phase diagram predicted for this model by the renormalization group used were described in I. Detailed numerical results for the fixed points in $d=2$ dimensions were presented and attention was focused on the renormalization-group description of the tricritical points for which the interaction parameters (J,D,H,H_3) provide the basis for a complete set of symmetry-breaking fields.[3]

In this paper the results presented in I are extended in two directions. First the dimensionality dependence of the fixed points and exponents is discussed. An expansion[4] in powers of $\epsilon=d-1$ is shown to provide a link between the exact results[5] for dimension $d=1$ and the approximate results for higher dimensions. The predicted variation with dimension of the tricritical exponents is investigated and is found to be somewhat surprising in that for some exponents it is not at all smooth.

Second a "dilution field"[6] is introduced into the Hamiltonian. This provides a free parameter which can be adjusted to provide recursion relations which are expected to yield an improved quantitative description of real systems near a two-dimensional tricritical point. Using these recursion relations various thermodynamic functions are evaluated. In particular, the three-phase monohedron,[7–9] which provides the basic representation of the thermodynamic densities at points of three-phase coexistence, is discussed. The problems involved in pursuing a similar approach for three-dimensional systems are outlined.

For convenience we recapitulate briefly the relevant notation and symmetry properties of the spin-1 model described in I. The spin-1 model is equivalent to a three-component lattice gas and the latter description was predominantly utilized in I. Here it is more convenient to work in terms of the magnetic Hamiltonian (1.1). Note first that (1.1) maps onto the same form under any permutation of the three spin states. For certain subspaces of the five-dimensional parameter space (J,K,D,H,H_3) the Hamiltonian is invariant under some or all of these permutations. Those which will be referred to here

are the three-dimensional *even subspaces,* namely,

$$H = H_3 = 0 \ , \tag{1.2}$$

$$3J - K + H_3 = 0, \quad 2H + H_3 - 2D + J + K = 0 \ , \tag{1.3}$$

$$3J - K - H_3 = 0, \quad 2H + H_3 + 2D - J - K = 0 \ , \tag{1.4}$$

which remain invariant under $(1,0,-1) \leftrightarrow (-1,0,1)$, $(1,0,-1) \leftrightarrow (0,1,-1)$, and $(1,0,-1) \leftrightarrow (1,-1,0)$, respectively, and the one-dimensional *Potts subspace,* namely,

$$H = H_3 = 0, \quad K = 3J, \quad D = 2J \ , \tag{1.5}$$

invariant under any permutation of the spin states. The Migdal-Kadanoff recursion scheme considered in I preserves the three-state permutation symmetry and hence the subspaces listed above are closed under the renormalization-group flows. It is helpful to remember that, as a consequence of the three-state permutation symmetry, fixed points in general occur in equivalence classes consisting of six fixed points with identical exponents. Fixed points in the even subspaces, however, occur in equivalence classes of three fixed points, those on the Potts line occur only once.

We follow the Griffiths thermodynamic notation employed in I where A^2 and A^3 denote manifolds of two- and three-phase coexistence, respectively, while B, BA, C, and Y denote critical, critical end point, tricritical, and three-state Potts manifolds, respectively. To distinguish fixed points from manifolds the relevant symbol is enclosed in angular brackets; for example $\langle C \rangle$ denotes a tricritical fixed point. Fixed points belonging to the same equivalence class are distinguished by subscripts α, β, γ, for those points lying within the even subspaces: otherwise by $\alpha\beta$, $\beta\gamma$, ...

The fixed points obtained are listed in Sec. II where properties of the renormalization-group transformation for $d = 1 + \epsilon$ dimensions are discussed. The notation used is

$$\bar{a} = \tfrac{1}{2}(J + K - H_3), \quad \bar{b} = \tfrac{1}{2}(J + K + H_3), \quad \bar{c} = 2J \ , \tag{1.6}$$

$$\zeta_a/\zeta_b = \exp(2H + H_3) \ ,$$

$$\zeta_b/\zeta_c = \exp[-D - H + \tfrac{1}{2}(J + K - H_3)] \ , \tag{1.7}$$

$$\zeta_a + \zeta_b + \zeta_c = 1 \ .$$

This notation is chosen to reflect the symmetries of the spin-1 model in that all fixed points within an equivalence class can be listed by simultaneous permutation of the fixed-point labels and of both the sets of coordinates, $\bar{a}$, $\bar{b}$, $\bar{c}$ and ζ_a, ζ_b, ζ_c.

The Migdal-Kadanoff-type renormalization scheme considered here[1] comprises two steps: (i) bond moving; and (ii) a one-dimensional exact decimation or dedecoration. On-site terms are divided equally among the q bonds incident upon a site and moved with those bonds[10]; this choice is advantageous because it yields exact results for ground-state energies. The steps (i) and (ii) may be performed in either order yielding two different approximations. The predicted *exponents* are independent of the order, as is the fixed-point topology. However, the fixed-point values in terms of (J,K,D,H,H_3) differ between the two schemes by a factor b^{d-1}. Hence there is a quantitative difference in the phase diagrams predicted. For example, the tricritical point coordinates for $K = 0$ are $(D = 2.13,\ J/q = 1.08)$ for the implementation [(i),(ii)] but $(D = 4.26,\ J/q = 2.15)$ for the implementation [(ii),(i)]. A comparison with previous estimates (I; Table V) suggests that the two results bound the exact value. As $b \to 1$ the two schemes become identical and better quantitative results are expected at the expense of increased numerical complexity. In I and Secs. II and III of this paper the sequence [(i),(ii)] was adhered to; the results presented in Secs. IV and V follow from the sequence [(ii),(i)]. Our primary interest is in the asymptotic equation of state which should be universal and hence independent of the quantitative features of the phase diagram. Thus we need not be too concerned by the differences. There is no direct evidence for preferring a particular order of implementation within the Migdal-Kadanoff scheme. Furthermore, the fact that both schemes are exact for a particular realizable system (see Appendix),[1,11] albeit without the usual translational invariance, should be borne in mind.

The layout of the paper is as follows. In Sec. II the expansion in ϵ with $d = 1 + \epsilon$ is discussed. As the fixed-point topology is identical for $d = 1 + \epsilon$ and $d = 2$ dimensions this provides a review of the most important results obtained in I. In Sec. III the dimensionality dependence of the fixed-point exponents is presented. The dilution parameter is introduced in Sec. IV and its effect on exponents and phase diagrams discussed. Section V concerns the thermodynamic densities and predictions for the shape of the three-phase monohedron in two dimensions. The Appendix discusses the realizability of the Migdal-Kadanoff scheme, particularly with respect to the introduction of dilution fields.

II. $1 + \epsilon$ EXPANSION

Krinsky and Furman[5] have provided an exact solution of the spin-1 model for dimension $d = 1$ using the transfer matrix technique. In particular these authors have listed the fixed points occurring for $d = 1$. An expansion in $\epsilon = d - 1$ about these fixed points provides a bridge between the exact one-dimensional results and the results obtained in I for $d = 2$. Indeed, the fixed-point topology found originally for

TABLE I. *Fixed points for $d = 1 + \epsilon$ related to the critical fixed points and the three-state Potts fixed point for $d = 1$.* Results exact to all orders in ϵ are starred. The notation introduced in I is followed.

	$\langle A^2\rangle^0_\gamma$	$\langle B\rangle^0_\gamma$	$\langle A^2\rangle_\gamma$	$\langle B\rangle_\gamma$	$\langle A^2\rangle_{\gamma\alpha}$	$\langle B\rangle_{\gamma\alpha}$
ζ_a	$\frac{1}{4}$	$\frac{1}{4}$	$\frac{1}{2}^*$	$\frac{1}{2}^*$	$\frac{1}{2}^*$	$\frac{1}{2}^*$
ζ_b	$\frac{1}{4}$	$\frac{1}{4}$	$\frac{1}{2}^*$	$\frac{1}{2}^*$	$\frac{1}{2}^*$	$\frac{1}{2}^*$
ζ_c	$\frac{1}{2}$	$\frac{1}{2}$	0^*	0^*	0^*	0^*
$\bar{a}/q$	∞^*	ϵ^{-1}	$\frac{1}{2}\ln 2^*$	$\frac{1}{2}\ln 2$	0^*	0^*
$\bar{b}/q$	∞^*	ϵ^{-1}	$\frac{1}{2}\ln 2^*$	$\frac{1}{2}\ln 2$	∞^*	ϵ^{-1}
$\bar{c}/q$	0^*	0^*	∞^*	ϵ^{-1}	∞^*	ϵ^{-1}

	$\langle A^3\rangle$	$\langle BA\rangle_\gamma$[a]	$\langle C\rangle_\gamma$	$\langle Y\rangle$
ζ_a	$\frac{1}{3}^*$	$\frac{1}{3}$	$\frac{1}{3}$	$\frac{1}{3}^*$
ζ_b	$\frac{1}{3}^*$	$\frac{1}{3}$	$\frac{1}{3}$	$\frac{1}{3}^*$
ζ_c	$\frac{1}{3}^*$	$\frac{1}{3}$	$\frac{1}{3}$	$\frac{1}{3}^*$
$\bar{a}/q$	∞^*	∞^*	ϵ^{-1}	ϵ^{-1}
$\bar{b}/q$	∞^*	∞^*	ϵ^{-1}	ϵ^{-1}
$\bar{c}/q$	∞^*	ϵ^{-1}	∞	ϵ^{-1}

[a]Degenerate with $\langle BA\rangle_{\gamma\alpha}$.

$d = 1 + \epsilon$ persists through all higher dimensions.

To illustrate the $1 + \epsilon$ expansion consider a Migdal-Kadanoff-type recursion relation[2] for the d-dimensional, spin-$\frac{1}{2}$ Ising model in zero field, namely

$$x' = \frac{2x^{2^{d-1}}}{1 + x^{4^{d-1}}}, \quad x = e^{-2J/k_B T} . \tag{2.1}$$

Here J is the usual, ferromagnetic nearest-neighbor interaction. For $d = 1$, fixed points $x^* = 0, 1$ ($T^* = 0, \infty$) describe a critical transition at zero temperature and a high-temperature sink, respectively. Recall that $d = 1$ is the lower critical dimension for the Ising model; when $d > 1$ the critical transition occurs at nonzero temperature. For $d = 1 + \epsilon$ fixed points occur at $x^* = 0$ ($T^* = 0$, low-temperature sink), $x^* = e^{-1/\epsilon}$ (critical) and $x^* = 1$ (high-temperature sink). Thus the critical fixed point at zero temperature for $d = 1$ bifurcates into a critical fixed point at nonzero temperature and a residual low-temperature sink which, on introducing a field, is seen to describe the expected first-order transition.

All the critical fixed points in the spin-1 model behave identically bifurcating, for $d = 1 + \epsilon$, into a critical fixed point which moves away from zero temperature as ϵ is increased and a residual first-order fixed point. These are listed in Table I. As in I, only one fixed point from each equivalence class is listed in the table. It is useful in understanding the connectivity of the phase diagram to note that the fixed points describing a first-order surface and its bounding critical line form a natural pair for $d = 1 + \epsilon$.

A three-state Potts fixed point $\langle Y\rangle$ is also found for $d = 1$ dimension. This exhibits more complicated behavior as illustrated in Fig. 1. When ϵ becomes positive this fixed point splits into a cube of 8 fixed points with one vertex fixed at the origin while the

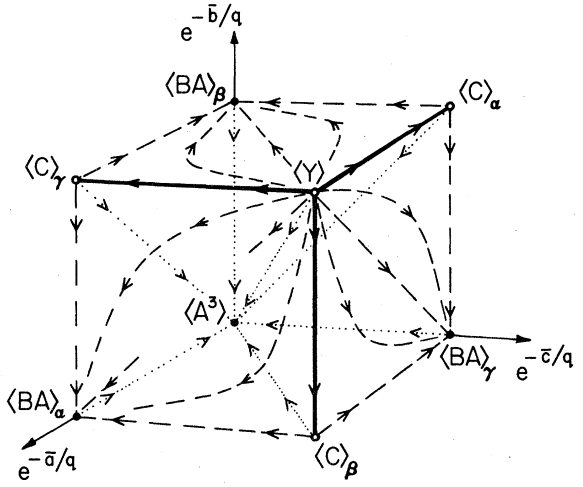

FIG. 1. Fixed points in dimension $d = 1 + \epsilon$ which spring from the Potts fixed point in $d = 1$. Note the three-state permutation symmetry about the line joining the Potts fixed point $\langle Y\rangle$ and the three-phase fixed point $\langle A^3\rangle$. The tricritical lines terminating at the tricritical fixed points $\langle C\rangle_\alpha$, $\langle C\rangle_\beta$, and $\langle C\rangle_\gamma$, the critical end-point surfaces, and the three-dimensional manifold of triple points are indicated schematically by solid, broken, and dotted lines, respectively.

TABLE II. *Critical exponents for dimension* $d = 1 + \epsilon$. Results exact to all orders in ϵ are starred.

Fixed Point	y_2	y_4	y_6	y_1	y_3
$\langle Y \rangle$	ϵ	ϵ	ϵ	$1+\epsilon$	ϵ
$\langle C \rangle_\gamma$	$1+\epsilon$	ϵ	$-1+\epsilon(1-\ln 2)$	$1+\epsilon$	ϵ
$\langle B \rangle_\gamma^0$	ϵ	$1+\epsilon$	$-\infty$	ϵ^*	$-1+\epsilon$
$\langle B \rangle_\gamma$	ϵ	$-\infty$	$-\infty$	$1+\epsilon$	ϵ
$\langle B \rangle_{\gamma\alpha}$	ϵ	$-\infty$	$-\infty$	$1+\epsilon$	$-1+\epsilon$
$\langle BA \rangle_\gamma$	ϵ	$1+\epsilon^*$	$-\infty$	$1+\epsilon$	ϵ
$\langle BA \rangle_{\gamma\alpha}$	ϵ	$1+\epsilon^*$	$-\infty$	$1+\epsilon$	$-2+\epsilon$

body diagonal through this vertex lies on the Potts line. The invariant point, $\langle A^3 \rangle$, becomes the triple point for $d > 1$ and the opposite vertex the three-state Potts point $\langle Y \rangle$. Of the remaining vertices three represent the critical end points, $\langle AB \rangle_\gamma$, (and their satellites,[1] $\langle AB \rangle_{\gamma\alpha}$, which occur at the same position in parameter space with the choice of variables used in the table) and three the tricritical points, $\langle C \rangle_\gamma$. These fixed points are listed in Table I. The connectivity under renormalization-group flows of the higher-order fixed points, which persists through all higher dimensions, is most easily calculated for $d = 1 + \epsilon$ and is depicted in Fig. 1. Note that this figure illustrates the three-state permutation symmetry of the spin-1 model around the Potts line as axis.

Table II lists the exponents of the fixed points for $d = 1 + \epsilon$. Fixed points within the same equivalence class have identical exponents and are therefore listed only once. In the majority of cases the first-order predictions agree well with the numerical results for the critical exponents for $d \lesssim 1.6$ (see Fig. 2). Results which are exact to all orders in ϵ for $d = 1 + \epsilon$ and hence which can be used to predict numerical values for higher dimensions, are starred in Tables I and II.

III. GENERAL DIMENSIONS

The fixed-point structure obtained in $1 + \epsilon$ dimensions persists through all higher dimensions. Thus, although it is very plausible that the renormalization-group described here predicts the true phase diagram in low dimensions, the results obtained differ significantly from those predicted by mean-field theory[12] (see also the discussion in I) which is expected to be correct for higher dimensionalities. In particular, the upper borderline dimensionality for tricritical behavior is $d = 3$: For $d > 3$ the tricritical exponents remain constant and equal to their mean-field value.[9,13–15] Within a renormalization-group context dimensionality expansions in the region of the borderline dimensionality suggest that this should be described by the tricritical fixed-point crossing and exchanging stability with a Gaussian fixed point.[16] Such a fixed point does not appear within the truncated parameter space used in the present approximate real-space renormalization group. Indeed a fixed-point structure describing the crossover to mean-field behavior as the dimension is increased has not, to our knowledge, been observed in real-space renormalization-group calculations, even for simple spin-$\frac{1}{2}$ Ising systems.

In the following section we introduce an additional field into the Hamiltonian which can be adjusted to "tune" exponents to give good agreement with exact and conjectured[17] results for $d = 2$. However, the dimensionality, d, itself appears as a free parameter in the recursion equations and it is therefore interesting to discuss first the dependence of the exponents on d. The results prove somewhat surprising.

Figure 2 shows the variation with d of the tricritical exponents or eigenvalues

$$y_i = (\ln \Lambda_i)/\ln b \quad , \tag{3.1}$$

where $b\,(=2)$ is the rescaling factor of the renormalization-group transformation and Λ_i denotes an eigenvalue of the recursion equations, I(3.2) and I(3.3), linearized about the appropriate fixed point. Results from the $1 + \epsilon$ and $3 - \epsilon$ expansions,[4,16] from the best previous real-space renormalization-group calculations[18,19] and from conjectures for the leading thermal and magnetic eigenvalues[17] are shown for comparison. The leading thermal, y_2, and magnetic, y_1, eigenvalues are in good agreement with exact and conjectured results in both two and three dimensions. Other eigenvalues are, however, represented rather poorly by the transformation. This suggests that numerical calculations of thermodynamic properties in the tricritical region on the basis of these recursion relations should be interpreted with caution and motivates the introduction of the dilution field in the next section.

The behavior of the plots between $d = 2$ and $d = 3$ dimensions deserves comment. For $d \simeq 2.2$ the

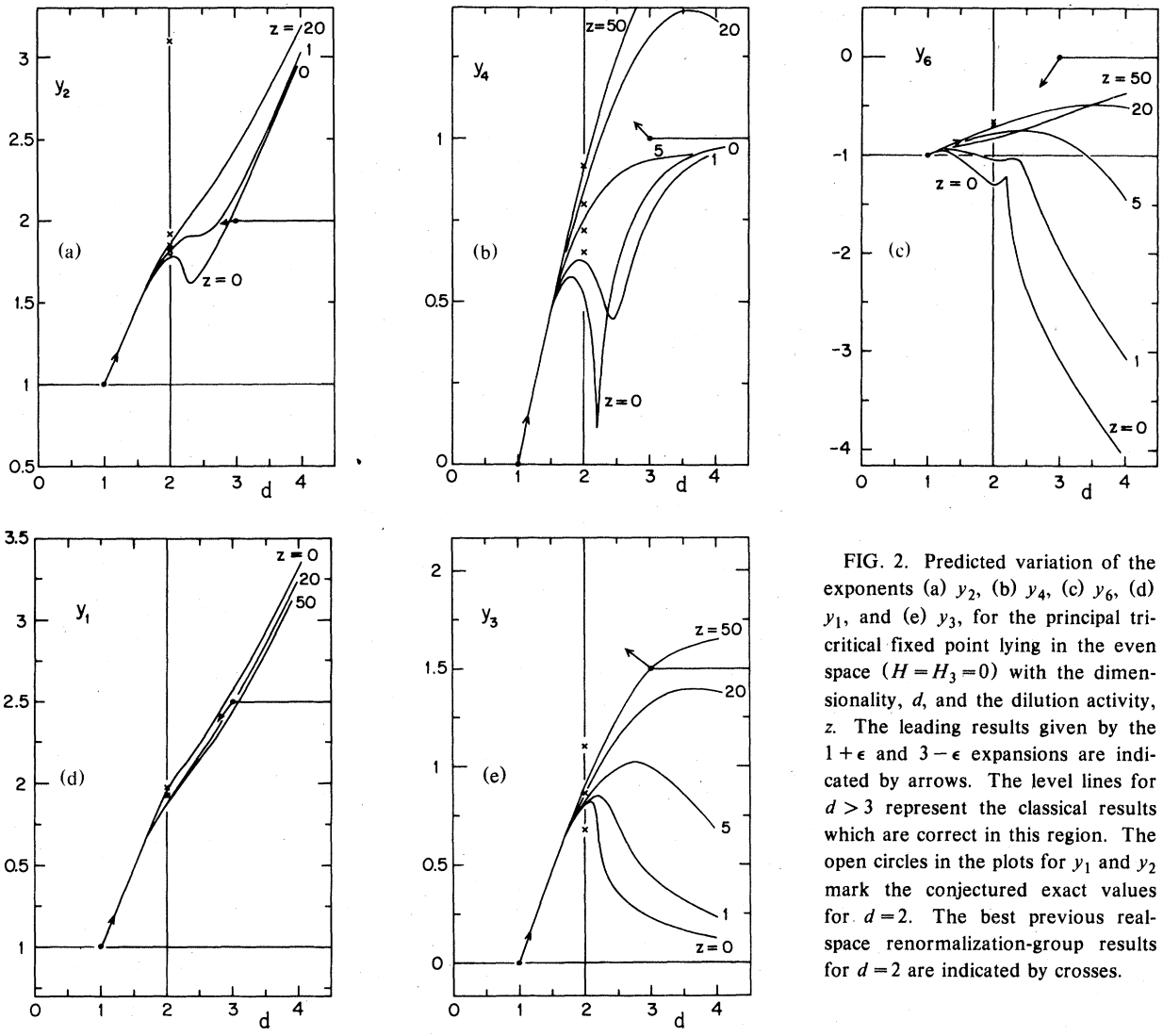

FIG. 2. Predicted variation of the exponents (a) y_2, (b) y_4, (c) y_6, (d) y_1, and (e) y_3, for the principal tricritical fixed point lying in the even space ($H = H_3 = 0$) with the dimensionality, d, and the dilution activity, z. The leading results given by the $1+\epsilon$ and $3-\epsilon$ expansions are indicated by arrows. The level lines for $d > 3$ represent the classical results which are correct in this region. The open circles in the plots for y_1 and y_2 mark the conjectured exact values for $d = 2$. The best previous real-space renormalization-group results for $d = 2$ are indicated by crosses.

second even eigenvalue, y_4, exhibits an extremely sharp minimum which is mirrored in the behavior of the other eigenvalues. A closer investigation of this region indicates that the "kinks" in the exponent graphs are not actually singularities, as they appear to be on the scale of Fig. 2, but rather are only rapid changes in slope, occurring at slightly different values of d for each exponent. The exponents behave in this way because the motion of the tricritical fixed point with d changes direction rather sharply within the five-dimensional parameter space at $d = d_0 \simeq 2.195$. One would expect this to be a consequence of the close approach of another fixed point repelling the first, as in the variation of the eigenvalues of a matrix. No such fixed point exists within the real physical parameter space, but a conjugate pair of complex fixed points do approach the tricritical fixed point sufficiently closely to affect its behavior. *A priori* it seems unlikely that this sharp behavior represents the true variation of the eigenvalues and exponents of the spin-1 Hamiltonian appropriately continued to arbitrary dimensionality. However, it is interesting to recall that our Migdal-Kadanoff-type recursion relations are exact for a realizable, albeit nontranslationally invariant, lattice.[11] We may note, however, that the eigenvalues of all other fixed points vary smoothly with dimensionality throughout the range, $d = 1$ to 4, examined. Furthermore, the dilution, to be introduced in the next section, can be adjusted to give a smoother variation of the tricritical exponents with d, together with more believable values of the exponents for $d = 2$ and 3 dimensions.

IV. INTRODUCTION OF A DILUTION FIELD

Let us now attempt to introduce a new parameter into the Hamiltonian (other than the dimensionality,

d) which might be adjusted to yield values for critical exponents in better agreement with the exact, conjectural, and other approximate but reliable results. If the recursion relations for the new model are still exact for some suitable pseudo-lattice structure,[11] they should provide a thermodynamically sensible description of behavior near tricritical points in real systems that will also, by adjustment, yield reasonably accurate exponents. To this end, consider a new local density, $t_i = 1, 0$, describing the concentration or dilution of the magnetically active sites,[6] and let the new Hamiltonian be

$$-\frac{\mathcal{H}}{k_B T} = H \sum_i s_i t_i - D \sum_i s_i^2 t_i - P \sum_i t_i + q^{-1} \sum_{\langle ij \rangle} [J s_i s_j + K s_i^2 s_j^2 + \tfrac{1}{2} H_3 s_i s_j (s_i + s_j)] t_i t_j \ , \quad (4.1)$$

where s_i takes the values 1, 0, and -1 as before when $t_i = 1$ but only, say, $s_i = 0$ when $t_i = 0$. The new field P is evidently the reduced chemical potential which controls the degree of dilution.

Now, for any fully translationally invariant lattice it is not hard to see that the effect of the dilution field P can be completely absorbed into the value of D in (1.1), since this field equally controls the density of sites in the state $s_i = 0$ (which are then effectively decoupled from the rest of the lattice). However, as we discuss in the Appendix, the hierarchical structures of the pseudo-lattices for which Migdal-Kadanoff recursion relations are exact,[11] allow freedom in the way the fields are assigned to the different levels of the hierarchy. The special properties of a dilution field in cases like this permit one to introduce P in such a way that it is *not* equivalent merely to a change in D but, nonetheless, still corresponds to a definite, realizable pseudo-lattice structure. Furthermore, we can arrange that P itself is a *renormalization-group invariant,* i.e., $P' = P$, while the recursion relations for the other parameters (J,K,D,H,H_3) depend parametrically on P (see Appendix). We then find that the overall fixed-point structure is almost identical for all values of P but the exponent values and the numerical details of the phase diagrams predicted by the new recursion relations, evolve with increasing P. This should be contrasted with the results obtained by Nienhuis, Berker, Riedel, and Schick[6] who first proposed the introduction of a dilution field. This enabled them to describe correctly the behavior of the q-state Potts model near $q = 4$. In their study the dilution variable provided an additional degree of freedom for flows within the parameter space and fixed points occurred only at specific values of the dilution field.

Note that only sites with $s_i = \pm 1$ are affected by the introduction of dilution; thus $s_i = 0$ becomes the increasingly favored local state. This is illustrated by Fig. 3 which shows a cross section of the phase boundary within the even space $H = H_3 = 0$ (D/J vs q/J for $K = 0$) for various values of the dilution field. For increasing $z = e^{2P/q}$ the Ising transition temperature in zero field moves to lower temperatures indicating that the spins $s_i = \pm 1$ are becoming more dilute and are therefore ordering less readily. Simultaneously the tricritical point moves to lower values of the field, D/J, indicating favoring of the zero-spin state. It follows that for $z \neq 0$ the three-state permutation symmetry of the model is broken. Note, however, that the inversion symmetry ($s_i \leftrightarrow -s_i$) is preserved. Thus the symmetry of the wings of the tricritical phase diagrams about the plane containing the lambda line is preserved only for the tricritical point lying in the even space $H = H_3 = 0$. The majority of the material presented in the remainder of this paper will pertain to this tricritical point which will be referred to as the principal tricritical point.

Figure 2 depicts the variation of the exponents of the principal tricritical point with dimensionality for chosen values of z. The leading thermal and magnetic exponents, y_2 and y_1, respectively, which were in good agreement with previous results[17,19] for $z = 0$ exhibit only a weak dependence on z. Values of the nonleading exponents, however, improve considerably as z is increased; in addition the exponent curves exhibit a much smoother variation with dimensionality. The choice $z = 20$ gives the best agreement with previous results[17,19] for $d = 2$ for all the tricritical exponents. To obtain a similar matching to the mean-field values for $d = 3$ the eigenvalue y_6 should become marginal. This would be expected to involve a change in the stability of the tricritical fixed point as

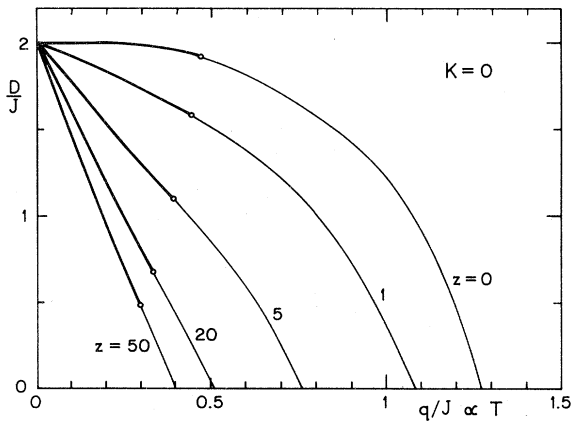

FIG. 3. The phase boundary of the three-component model in the even space ($H = H_3 = 0$) with $K = 0$ for various values of the dilution activity, z. The bold curves represent first-order phase boundaries while the thin curves depict the critical or lambda lines. The tricritical points are indicated by open circles.

TABLE III. *Fixed-point exponents for $d=2$ and $z=20$.* Fixed points controlling the phase diagram of the principal tricritical point are starred.

Fixed point		y_2	y_4	y_6	y_1	y_3
$\langle Y\rangle$		0.895	1.832	0.764	1.868	0.895
$\langle C\rangle_\gamma$	*	1.852	0.846	−0.726	1.867	0.862
$\langle C\rangle_\alpha, \langle C\rangle_\beta$		1.706	0.453	−2.270	1.960	0.903
$\langle B\rangle^0_\gamma$		0.820	1.864	$-\infty$	$1(\equiv d-1)$	0.209
$\langle B\rangle^0_\alpha, \langle B\rangle^0_\beta$	*	0.857	1.860	$-\infty$	1	−1.102
$\langle B\rangle_\gamma$	*	0.747	$-\infty$	$-\infty$	1.879	0.121
$\langle B\rangle_\alpha, \langle B\rangle_\beta$		0.855	$-\infty$	$-\infty$	1.860	0.321
$\langle B\rangle_{\gamma\alpha}, \langle B\rangle_{\gamma\beta}$	*	0.747	$-\infty$	$-\infty$	1.879	−0.253
$\langle B\rangle_{\alpha\gamma}, \langle B\rangle_{\beta\gamma}$		0.855	$-\infty$	$-\infty$	1.860	−0.555
$\langle B\rangle_{\alpha\beta}, \langle B\rangle_{\beta\alpha}$	*	0.855	$-\infty$	$-\infty$	1.860	−1.087
$\langle BA\rangle_\gamma$		0.747	$2(\equiv d)$	$-\infty$	1.879	0.782
$\langle BA\rangle_\alpha, \langle BA\rangle_\beta$		0.855	2	$-\infty$	1.860	0.449
$\langle BA\rangle_{\gamma\alpha}, \langle BA\rangle_{\gamma\beta}$		0.747	2	$-\infty$	1.879	−2.615
$\langle BA\rangle_{\alpha\gamma}, \langle BA\rangle_{\beta\gamma}$	*	0.855	2	$-\infty$	1.860	−0.719
$\langle BA\rangle_{\alpha\beta}, \langle BA\rangle_{\beta\alpha}$		0.855	2	$-\infty$	1.860	−2.613

d passes through $d=3$, which, for the principal tricritical point, does not occur for any values of z and d.

Table III lists the critical exponents of the fixed points for $d=2$ and $z=20$. Fixed points which describe the phase diagram of the principal tricritical point are indicated by an asterisk. The results should be compared to those for $z=0$ in I, Table III. The notation used in I is maintained but, due to the breaking of the three-state permutation symmetry, fixed points which belonged to the same equivalence class no longer have the same exponents. For the secondary tricritical points the exponents become less accurate with increasing z. Exponents of the critical and critical-end fixed points do not show a marked dependence on z with the exception of y_3. Variation of y_3 is much more strongly marked: for $\langle B\rangle^0_\alpha, \langle B\rangle^0_\beta$ it changes sign as z is increased indicating a change in the connectivity of the fixed points. This, however, does not affect the fixed-point topology describing the principal tricritical point.

To adjust the exponents it might seem easier to introduce free parameters directly into the recursion relations, rather than into the Hamiltonian. However, there would then be no guarantee that the resulting approximate recursion equations could generate a physically sensible, positive, convex free energy. Conversely the introduction of a dilution field, P or z, into the Hamiltonian leads to a renormalization-group scheme that is realizable in the sense of Berker[11] in that it describes exactly the behavior of a system with the Hamiltonian (4.1) on a special, hierarchically structured "lattice." A point worth noting, however, is the following: *a priori* the hypothesis of universality would suggest that the tricritical and critical exponents of such a lattice should not depend continuously on the dilution field (even if the exponents for $z\neq 0$ were different from those for $z>0$). The fact that z itself does not flow under the exact recursion relations for the model means that such universal behavior could occur only if the eigenvalues of the fixed points were z independent. As explained, however, this is not the case. This nonuniversal tricritical behavior does not seem physically plausible for $d<3$, indicating that the behavior of the Berker system differs substantially from that of real two- or three-dimensional lattice systems. (See also the results for various "fractal lattices" discussed by Gefen, Mandelbrot, and Aharony.[20])

V. THREE-PHASE MONOHEDRON

The three-phase monohedron, described by Griffiths,[7] Widom,[8] and others,[9] provides the representation of the thermodynamic densities at points of three-phase coexistence lying in the tricritical region of the phase diagram. It is by considering this figure that experimental results on the tricritical behavior of real, four-component fluid mixtures have been most directly displayed.[8] The general shape of the three-phase monohedron which emerges from the classical phenomenological or Landau theory is illustrated in

Fig. 4. At each temperature below tricriticality there is a line of points in the field space (D,H,H_3) with K fixed, describing three-phase coexistence and terminating at two critical end points. Each point on this triple line defines a triangle within the conjugate density space with coordinates

$$m_1=\langle s_i\rangle=\frac{\partial F}{\partial H},\quad m_2=\langle s_i^2\rangle=-\frac{\partial F}{\partial D}\ ,$$
$$m_3=\langle s_i^2 s_j\rangle=2\frac{\partial F}{\partial H_3}\ , \tag{5.1}$$

where s_i denotes a general spin with nearest neighbor s_j and $F=F(J,K,D,H,H_3)$ is the appropriate reduced free energy. Each vertex of the triangle in the space (m_1,m_2,m_3) describes the densities of the three corresponding coexisting phases. On moving along the triple line in the field space (D,H,H_3) a stack of contiguous coexistence triangles is built up in density space as illustrated in Fig. 4. Approaching the top or bottom of the stack corresponds to approaching one or other of the critical end points in field space; the coexistence triangles become narrower as the densities of the two phases which will achieve criticality become more nearly identical. The stack ends in the critical end-point tie lines E_-C_+ and E_+C_-. The vertices of the coexistence triangles form a curvilinear locus, $E_-O_-C_-OC_+O_+E_+$, in the three-dimensional density space (m_1,m_2,m_3), the *edge* of the three-phase monohedron. The sides of the three-phase triangles form the single continuous, smooth ruled *face* of the monohedron.

A similar monohedron may be constructed for each temperature less than the tricritical temperature, T_t. To specify the shape of the monohedron it is first appropriate to introduce the scaling densities which are, asymptotically, fixed linear combinations of the densities m_i. The symmetry under $s_i \leftrightarrow -s_i$ simplifies the form of these, and we may take

$$\tilde{m}_1=m_1,\quad \tilde{m}_2=m_2-m_{2,O}(T),$$
$$\tilde{m}_3=m_3-c(T)m_1\ , \tag{5.2}$$

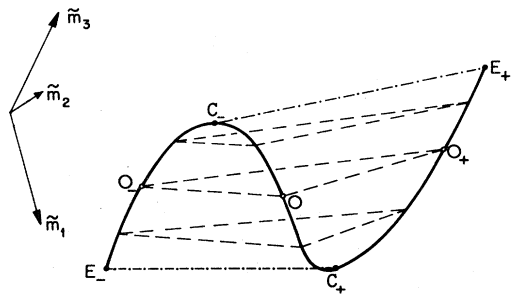

FIG. 4. A general view in the space of densities (m_1,m_2,m_3) of the three-phase monohedron as predicted by classical theory. Coexistence triangles, the vertices of which represent the densities of the three coexisting phases, are indicated by dashed lines. The points C_+ and C_- are critical points coexisting with noncritical phases E_- and E_+ and thus represent the critical end points. The "central point," O, is the point of asymptotic symmetry. The $\tilde{m}_j$ label the scaling densities and correspond to linear combinations of the densities m_i.

where the subscript O denotes the *central point* labeled O in Fig. 4, which corresponds to the symmetry plane $H=H_3=0$ and $m_1=m_3=0$: thus $m_{2,O}(T)$ is the value of m_2 in the disordered phase on the triple line at temperature T where it intersects the symmetry plane. The choice of the mixing parameter $c(T)$ will be explained shortly. If the reduced temperature deviation from tricriticality is defined, as usual, by

$$t=(T-T_t)/T_t=(J_t/J)-1\ , \tag{5.3}$$

the size of the monohedron shrinks as $t\to 0$ according to

$$\tilde{m}_{j,E+}\approx B_{j,E+}|t|^{\beta_j},\quad \beta_j=(d-y_j)/y_4\ , \tag{5.4}$$

for $j=1,2,3$, where the subscript $E+$ denotes the critical end point E_+ (see Fig. 4) which specifies the maximal extent of the monohedron (with respect to the central point O where $\tilde{m}_1=\tilde{m}_2=\tilde{m}_3=0$). Since $\beta_1>\beta_2>\beta_3$ (see Table IV) the monohedron shrinks

TABLE IV. *Exponents for the tricritical monohedron.* The overdot denotes the wing critical exponent.

	$\dot{\beta}$	β_1	β_2	β_3
Classical	$\frac{1}{2}$	$\frac{1}{2}$	1	$1\frac{1}{2}$
$d=2$				
$z=0$	0.162	0.122	0.437	2.29
$z=20$	0.164	0.157	0.175	1.34
Previous results	$\frac{1}{8}$ (exact)	0.077[a]	0.177[a]	1.23[a]
		0.091[b]	0.255[b]	1.12[b]
			0.227[c]	
		0.083±18[d]	0.24±4[d]	1.04±9[d]

[a]Reference 18.
[b]Reference 19.
[c]Reference 21.
[d]Reference 22.

as $t \to 0$ first to, asymptotically, a triangle, then to a line, and finally, at tricriticality, to a single point.

Our aim here is to characterize the three-phase monohedron for two-dimensional systems with the expectation or, at least, hope that experimental data will become available in the future for comparison with theory. However, to put our results in perspective and to bring out the somewhat peculiar nature of the monohedron it is useful to review briefly the results predicted by the classical phenomenological theory.[7–9] If we neglect logarithmic corrections,[13,14] which are probably small in this respect, and the effects of nonclassical critical behavior at the critical end points C_+ and C_-, which remains to be quantified, the phenomenological theory may be expected to describe three-dimensional systems correctly: indeed it accounts surprisingly well for the observations on four-component fluid mixtures.[8] The shapes of the monohedra are most easily assimilated and compared by looking at three canonical projections, namely, onto the three natural scaling planes defined by $\tilde{m}_3 = 0$, $\tilde{m}_2 = 0$, and $\tilde{m}_1 = 0$. It is also helpful to introduce the *reduced scaling densities*[9(b)]

$$w_j = \tilde{m}_j / B_{j,E+} |t|^{\beta_j}, \quad (j = 1, 2, 3) \ , \tag{5.5}$$

in terms of which the coordinates of the end points E_+ and E_- are simply $w_1 = \pm\, w_2 = w_3 = \pm 1$ (while the central point O is located at the origin $w_1 = w_2 = w_3 = 0$, and we assume odd or even symmetry under $w_j \leftrightarrow -w_j$, which is certainly correct when the tricritical point lies in a plane of spin inversion symmetry as in the cases we shall discuss).

The asymptotic shape of the monohedron as predicted by classical theory[7–9] is then specified by the projections of the edge as

$$w_2 = w_1^2, \quad (\text{parabolic}, \ \tilde{m}_3 = 0) \ , \tag{5.6}$$

$$w_3 = w_1^3, \quad (\text{cubic}, \ \tilde{m}_2 = 0) \ , \tag{5.7}$$

$$w_3 = \pm\, w_2^{3/2}, \quad (\text{cuspoidal}, \ \tilde{m}_1 = 0) \ . \tag{5.8}$$

These projections of the classical monohedron are represented by the dotted lines in Figs. 5(a), (b), and (c). The critical end-point phases C_+, E_-, C_-, and E_+ are indicated by small solid circles: the points O_+ and O_-, representing the phases coexisting with the central-point phase O (see Fig. 4), are located by small open circles. The descriptive names "parabolic," "cubic," and "cuspoidal" will be retained to designate the corresponding three projections of the monohedra also for two-dimensional systems even though, as will be seen, the plots are no longer perfect parabolas or cubic curves.

At this point it is also convenient to explain the specification of the cubic mixing coefficient, $c(T)$, in (5.2): this is chosen so that the slope of the cubic projection vanishes at the origin. As a function of temperature, this choice also serves to cancel out the strongly varying power $|t|^{\beta_1}$ from, say, $m_{3,E+}(T)$ to reveal the weaker scaling power $|t|^{\beta_3}$. The corresponding "rectification" of the monohedron can be specified similarly in situations lacking an exact spin inversion symmetry or its equivalent but the appropriate prescription is more complicated.

As discussed in connection with the infinite-component limit ($n \to \infty$) in a three-dimensional system,[9] where the shape of the monohedron may be quantified conveniently in terms of the dimensionless ratios

$$\mathfrak{R}_{O,j} = [O_+O]_j / [E_+O]_j \ , \tag{5.9}$$

$$\mathfrak{R}_{c,j} = [C_+O]_j / [E_+O]_j \ , \tag{5.10}$$

where, in general, $[PO]_j$ denotes the length of the line segment PO in density space when projected onto the $\tilde{m}_j$ (or w_j) axis. The values of the ratios predicted classically are listed in the first line of Table V.

We have studied the shape of the three-phase monohedron predicted for a two-dimensional system by the Migdal-Kadanoff-type recursion relations explained in I and by the modified recursion relations incorporating the dilution parameter described in Sec. IV above. In both cases we have utilized the sequence [(ii), (i)] which, as mentioned in Sec. I, is exact for a hierarchical lattice structure.[11] In the latter case attention has been confined to the principal tricritical point lying in the even subspace, $H = H_3 = 0$. For the dilution activity we have chosen the value $z = 20$, which, as evident from Fig. 2, reproduces the fixed-point exponents y_i with reasonably good overall accuracy. However, in the case of the size and shape of the monohedron the most important exponents are, first, the ordinary or "wing" critical point exponent

$$\dot{\beta} = (d - y_{1\langle B\rangle}) / y_{2\langle B\rangle} \ , \tag{5.11}$$

which describes behavior on the critical surfaces and *at* the critical end points; in particular, this exponent controls the degree of "flatness" of the edge of the monohedron around C_+ and C_-; and, second, the three tricritical exponents β_1, β_2, and β_3. The values of these exponents predicted classically, given by our recursion relations, and found, via (5.4) by previous calculations,[18,19,21,22] are listed in Table IV. In classical theory the ratios β_2/β_1 and β_3/β_2 are 2.0 and 1.5, respectively, which values indirectly reflect the parabolic and cuspoidal character of the projections. Two previous calculations,[18,19] yield $\beta_2/\beta_1 \simeq 2.30$, $\beta_3/\beta_2 \simeq 6.9$, and 2.80 and 4.4, respectively. The differences between the two sets of estimates probably provide a fair indication of their accuracy. Evidently the monohedron flattens to a triangle, and then to a line, more rapidly in two dimensions than in three. From our present recursion relations we find $\beta_2/\beta_1 \simeq 3.6$ and $\beta_3/\beta_2 \simeq 5.2$ for $z = 0$, and 1.1 and 7.7 for $z = 20$. A comparison with the earlier cal-

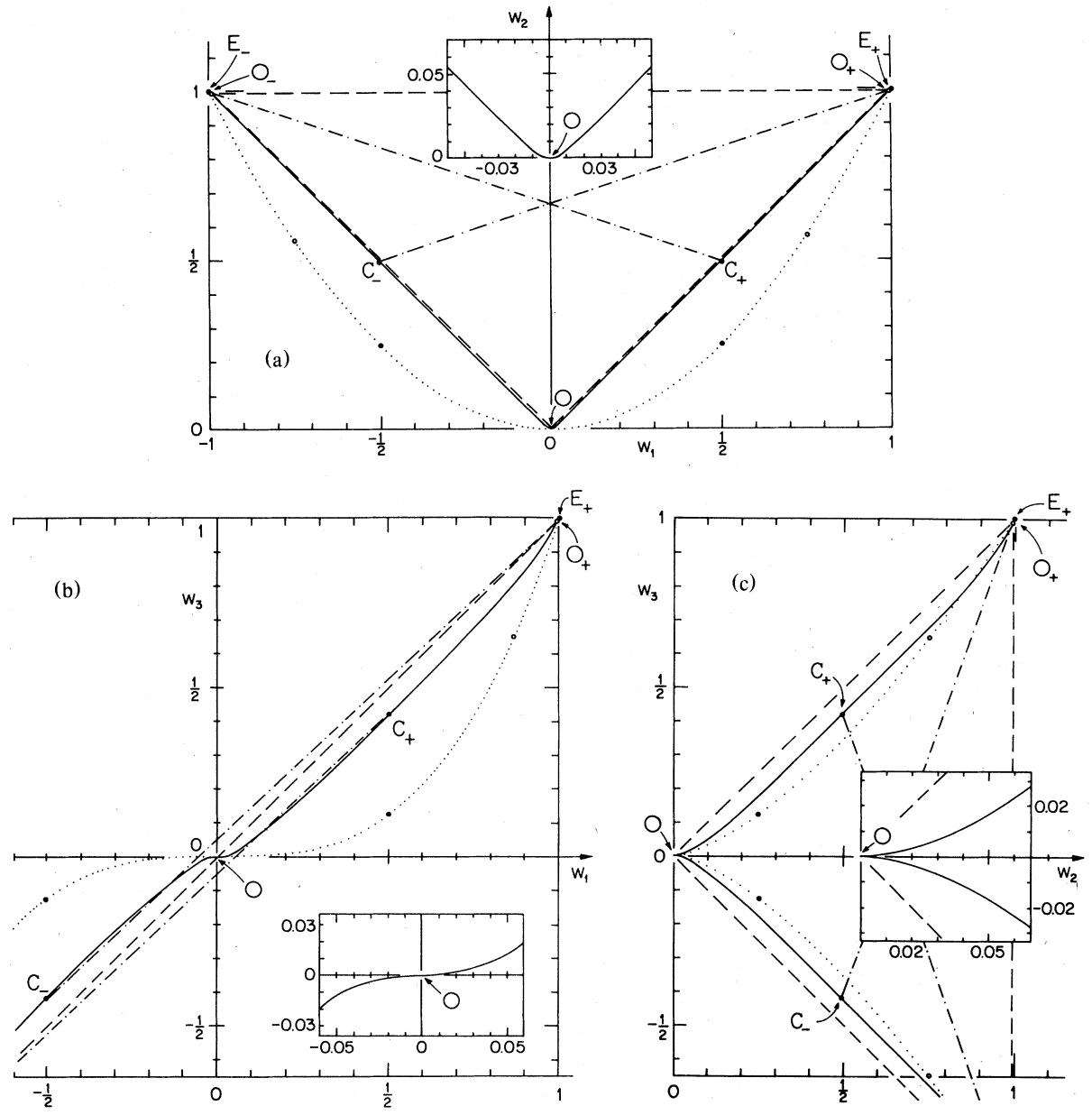

FIG. 5. Projections of the three-phase monohedron for $z=0$, $K=0$, and $q/J=0.20$ (or $T\simeq 0.43T_t$): (a) parabolic, (b) cubic, and (c) cuspoidal (solid curves). The predictions of classical theory are indicated by the dotted curves for comparison. The central coexistence triangle, O_+OO_-, and the critical end-point tie lines, C_+E_- and C_-E_+, are indicated by dashed and dot-dash lines, respectively (see also Fig. 4). The inset in each figure expands the region around the central point, O.

culations suggests that, in this respect, some intermediate value, say $z\simeq 5$ or 10, might represent a better compromise. However, inasfar as these ratios affect the shape of the monohedron—as indeed they appear to in some significant respects—it is reasonable to hope that the true behavior will be bracketed by the results for $z=0$ and $z=20$.

We have generated the monohedra by integrating the recursion relations for m_1, m_2, and m_3 at various temperatures for $z=0$ and $z=20$ with $K/J=0$ and $K/J=1$. The shape ratios $\mathcal{R}_{O,j}$ and $\mathcal{R}_{c,j}$ are presented in Table V for the monohedra considered in detail. The corresponding densities and mixing parameters needed to set the size and position of the monohedra are listed in Table VI. For $q/J=0.2$ which corresponds to a temperature of about 43% of T_t (see Fig. 3), and three projections of the monohedron for $K/J=0$ and $z=0$ are shown as the solid lines in

TABLE V. *Shape parameters for the three-phase monohedra.* The ratios $\mathfrak{R}_{O,J}$ and $\mathfrak{R}_{c,J}$ are defined through (5.9) and (5.10) with the aid of Fig. 4.

	$\mathfrak{R}_{O,1}$	$\mathfrak{R}_{O,2}$	$\mathfrak{R}_{O,3}$	$\mathfrak{R}_{c,1}$	$\mathfrak{R}_{c,2}$	$\mathfrak{R}_{c,3}$
Classical (Ref. 9)	$(3/4)^{1/2}$ $\simeq 0.866$	$\frac{3}{4}$	$(3/4)^{3/2}$ $\simeq 0.650$	$\frac{1}{2}$	$\frac{1}{4}$	$\frac{1}{8}$
$z=0,\ K=0$						
$q/J=0.20$	0.997	0.997	0.993	0.500	0.497	0.420
$=0.45$	0.947	0.930	0.845	0.50	0.43	0.33
$z=20,\ K=J$						
$q/J=0.20$	1.000	1.000	1.000	0.05	0.05	0.03
$z=20,\ K=0$						
$q/J=0.20$	0.990	0.990	0.981	0.048	0.046	0.028
$=0.332\,30$	0.86	0.86	0.83	$\lesssim 0.05$	$\lesssim 0.05$	$\lesssim 0.05$

Figs. 5(a), (b), and (c). The most striking ways in which this monohedron differs from the classical prediction are in its flatness, as seen in the cubic projection, and in the comparative straightness of the two "arms" of the edge. These features seem to be mainly a consequence of the large value of $1/\beta$ (which would be larger still in a more accurate representation of the Ising-like wing critical behavior). The characteristic, rounded, parabolic, and cubic aspects and the pointed cuspoidal shape of the projections of the monohedron become apparent only very near the central point O: see the insets in Fig. 5. The critical end points C_+ and C_- are indicated by solid circles. In the parabolic and cubic aspects these, together with the central point O, roughly quadrisect the edge of the monohedron, i.e., $\mathfrak{R}_{c,1}$ is close to the classical value $\frac{1}{2}$. However, as evident from Table V, $\mathfrak{R}_{c,2}$ and $\mathfrak{R}_{c,3}$ differ significantly from the classical values because of the straightness of the edges of the monohedron. Because T is, in this case, rather far below T_t, some distortion of the monohedron from its asymptotic tricritical shape is certainly expected since m_1 and m_2 are close to their saturation values (see Table V): this is the reason the ratios $R_{O,J}$, which locate the points O_+ and O_- (open circles in Fig. 5), are so close to unity. However, even for $q/J=0.45$, which corresponds to $|t|\simeq 0.03$, the value of $\mathfrak{R}_{O,1}$ has dropped only to 0.947, which is 9% higher than the classical result. The values of $\mathfrak{R}_{O,2}$, $\mathfrak{R}_{O,3}$, $\mathfrak{R}_{c,2}$, and $\mathfrak{R}_{c,3}$ are also smaller than at low T, so that the monohedron close to tricriticality is slightly less flattened with respect to classical predictions: however, the overall appearance is still not very different from that illustrated in Fig. 5.

For $z=20$ and $q/J=0.2$ the monohedron was constructed for $K/J=1$ as well as for $K/J=0$, in order

TABLE VI. *Size parameters for the three-phase monohedron for $K=0$.* See (5.1) and (5.2) for the definition of the scaled densities, etc.

z	q/J	$\tilde{m}_{1,E+}$	$\tilde{m}_{2,E+}$	$\tilde{m}_{3,E+}$	$m_{2,O}$	$c(T)$
0	0.20	0.9998	0.9924	0.9095	0.007 36	0.090
	0.45	0.7965	0.4268	0.0270	0.3934	0.8834
20	0.20	0.9987	0.9960	0.9204	0.002 66	0.077
	0.332 30	0.3620	0.3115	0.002 24	0.0849	0.862

to test the sensitivity of the shape to an irrelevant variable. Note that the same tricritical fixed point controls the shape of the monohedron for all K, so that the asymptotic shape close to tricriticality is certainly universal for fixed z. As confirmed by Table V the shapes are scarcely affected by the value of K even at such a large deviation from tricriticality. (For $z=20$ one has $q/J_t \simeq 0.332\,33$.) A surprising feature, however, is the small value of the ratios $\mathcal{R}_{c,J}$, which imply that the critical end points, C_+ and C_-, are now very close to the central point O. This feature of the monohedra remains even for $q/J = 0.332\,30$, corresponding to $|t| \simeq 10^{-4}$, as can be seen from Table V and the projections plotted in Figs. 6(a), (b), and (c). These plots again exhibit the striking flatness of the monohedron and the straightness of the two arms of the edge.

The data reported in Table V and Figs. 5 and 6 suggest that the flatness of the monohedra is a true feature of tricriticality in two-dimensional systems. If the degree of flatness is measured by $\mathcal{F}$, the maximum departure of the scaled cubic projection of the

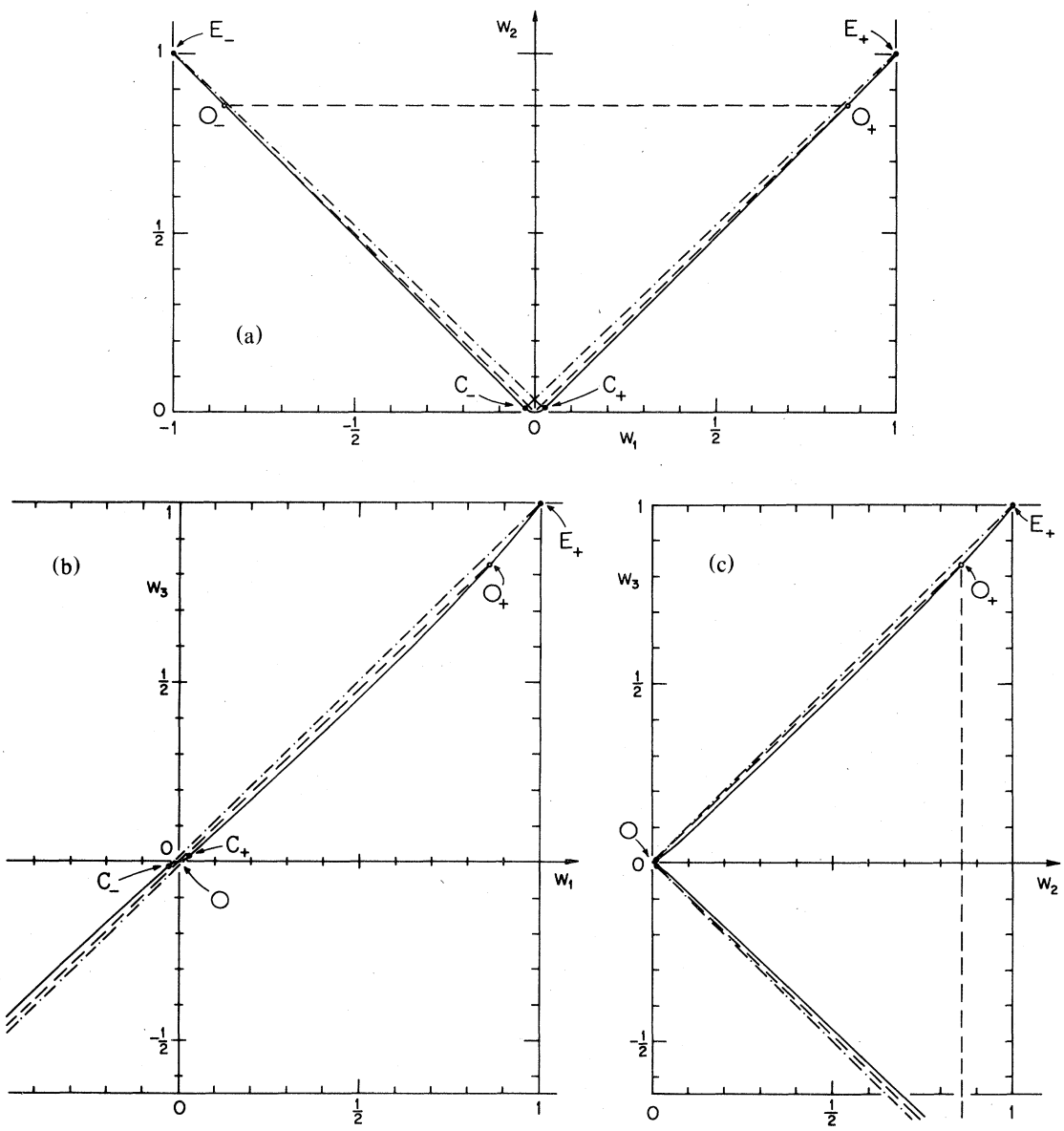

FIG. 6. Projections of the three-phase monohedron for $z=20$, $K=0$, and $q/J=0.332\,30$ (corresponding to $|t| \simeq 10^{-4}$). As in Fig. 5 the edge of the monohedron is shown as a solid curve; the central coexistence triangle, O_+OO_-, and the critical endpoint tie lines, C_+E_- and C_-E_+, are indicated by dashed and dot-dash lines, respectively.

edge of the monohedron from the diagonal $w_3 = w_1$, one finds $\mathfrak{T} = \frac{1}{3}(\frac{2}{3})^{1/2} \simeq 0.272$ for classical theory, whereas our calculations close to tricriticality yield, for $d = 2$, $\mathfrak{T} \simeq 0.12$ when $z = 0$ and $\mathfrak{T} \simeq 0.03$ when $z = 20$. As suggested in discussing the value of the exponents β_j, the true value of $\mathfrak{T}$ is probably bracketed by these estimates. The asymptotic positions of the points O_+ and O_-, representing the phases coexisting with the symmetric, central phase at O, are probably also bracketed by the values of $\mathfrak{R}_{O,j}$ in Table V. We conclude that they lie somewhat closer to the end points E_+ and E_- than classically predicted, say with $\mathfrak{R}_{O,1} \simeq 0.90$ in place of 0.866.

However, the true location of the critical end points C_+ and C_- is more problematical. As noted before, the value of $\mathfrak{R}_{c,1}$ for $z = 0$ is close to the classical result $\frac{1}{2}$; however, for $z = 20$ values of 0.05 or smaller are found. (The lack of precision in the last-row values for the $\mathfrak{R}_{c,j}$ in Table V arises from the accumulation of roundoff errors in the iterations, which becomes severe for small t, particularly near the critical end points where two fixed points compete.) While it is certainly reasonable to guess that the true position of the critical end points lies between these extremes, it is clear that a further study using a more accurate renormalization-group approximation with a larger parameter space is needed to derive any more useful and convincing estimate! Despite the unexpected sensitivity of this aspect of the tricritical monohedron to the value of the dilution parameter, we do feel that the flatness of the monohedron in two dimensions and the estimates for the $O_\pm$ points are trustworthy.

A final point deserves comment, namely, the extent of the asymptotic tricritical region. Since the exponent β_1 is rather small, the value of m_1 even very close to the tricritical point remains quite large (see Table VI), and one may reasonably doubt that the monohedra studied are close enough to tricriticality to represent the desired asymptotic forms accurately. To the extent that the numerical results are more sensitive to the value of the dilution activity z than to the temperature, the question is somewhat academic. Nevertheless, it is conveniently answered by using the values of β_1 and β_2, as calculated directly from the linearized recursion relations at the tricritical fixed point, to fit the functions $\tilde{m}_{1,O+}(T)$ and $\tilde{m}_{2,O+}(T)$, which are fairly easy to compute accurately. For $z = 20$ the form

$$\tilde{m}_{1,O+} \simeq B_{1,O+}|t|^{\beta_1}[1 + b_1 t] \ , \tag{5.12}$$

and its analog for $\tilde{m}_2$, yields a good fit near T_t with $B_{1,O+} \simeq 1.303 \pm 7$, $b_1 \simeq 0.61$, and $B_{2,O+} \simeq 1.315 \pm 8$, $b_2 \simeq 0.57$ (the uncertainties referring to the last decimal place). The relatively small values of the correction amplitudes show that the monohedra are probably quite close to their asymptotic forms for T within 2 or 3% of T_t. Since the leading correction to scaling exponent, y_6, is moderately large at $d = 2$, this conclusion is probably also correct for real systems.

VI. SUMMARY AND CONCLUSIONS

To conclude, a brief summary of the main results obtained is in order. In Part I[1] a Migdal-Kadanoff-type recursion relation[2] was applied to a general spin-1 Ising model. The resulting global phase diagram was elucidated for $d = 2$ dimensions. In this part general dimensionality, d, has been considered. The renormalization-group fixed-point structure is found to be identical for all values of d; a brief discussion of the consequent failure of this renormalization group to predict a crossover to mean-field behavior for $d = 3$ or 4 was presented. This problem is general for real-space renormalization-group schemes and deserves further attention. Results for $d = 1 + \epsilon$ with ϵ small have been found to provide a numerically useful link to the exact results available for $d = 1$. The behavior of the tricritical exponents as a function of dimensionality is surprisingly irregular for $d \simeq 2.2$, a phenomenon found to reflect a sensitivity to the close approach of nonphysical fixed points lying within the complex plane. This indicates the circumspection with which results obtained from real-space renormalization-group calculations should be evaluated.

A dilution field introduced into the Hamiltonian may be adjusted to tune the tricritical exponents to better agree with previously calculated and conjectured values for $d = 2$.[17–19] Using the original and modified recursion relations the characteristics of the three-phase monohedron have been studied. Significant differences from classical theory are predicted: the monohedron is almost "flat," except very close to the origin, and the points O_+ and O_-, coexisting with the central or symmetry point O, lie close to the limiting end points E_+ and E_- (see Fig. 4 and Table V). It is encouraging that the leading tricritical exponents, which agree quite well with conjectured results, and the overall shape of the monohedra depend only fairly weakly on the added dilution field. However, the nonleading tricritical exponents and, especially, the relative positions of the critical end points depend strongly on the degree of dilution. These parameters should be universal quantities and such dependence on a simple property of the Hamiltonian highlights the inadequacies of the simple Migdal-Kadanoff type of renormalization-group schemes. It should be recalled, however, that, as demonstrated in the Appendix, the renormalization-group schemes employed here are exact for Berker-type hierarchical lattices[11]: thus our calculations expose the degree of nonuniversality displayed by such nontranslationally invariant (or fractal[20]) systems.

And, finally, our calculations provide some support for the hope that, by using the freedom to adjust the exponents to take optimal values, the asymptotic thermodynamic functions may be predicted more reliably.

ACKNOWLEDGMENTS

We are grateful to Dr. Stellan Ostlund for help and advice in setting up the numerical calculations and indebted to Dr. Miron Kaufman for pointing out a mistake in our first draft. The support of the National Science Foundation through the Materials Science Center at Cornell University is gratefully acknowledged.

APPENDIX: REALIZATION OF THE MIGDAL-KADANOFF RECURSION RELATIONS ON A HIERARCHICAL LATTICE AND THE INTRODUCTION OF FIELDS

As pointed out by Berker (see also Forgács),[11] one can construct special hierarchically structured lattices or pseudo-lattices for which recursion relations of the Migdal-Kadanoff type constitute an *exact* renormalization group. Here we discuss the renormalization-group transformation of such pseudo-lattices under the Migdal-Kadanoff scheme with particular reference to single-site or field terms. Thereby we will motivate the recursion equations utilized in Secs. IV and V for the Hamiltonian (4.1), (describing the spin-1 model with a "dilution" field) and establish their realizability.

The particular hierachical lattice structure which realizes the two-step Migdal-Kadanoff scheme of one-dimensional decimation or dedecoration[23] followed by a bond-moving transformation, is most easily visualized by starting from a single bond and iterating the renormalization group in reverse. (The same procedure may be used for the alternative scheme [(i), (ii)] discussed in Sec. I.) In the (approximate) application to a d-dimensional hypercubic lattice with a renormalization of the linear scale by a factor b, the bond-moving step groups a set of $p = b^{d-1}$ parallel bonds to form a single new, renormalized bond. Thus on reversing the process the single starting bond is replaced by a set of p equal, parallel bonds linking the two original terminal sites. Reversal of the decimation step then corresponds to decorating each of the p parallel bonds with $(b-1)$ new sites coupled equally in linear sequence resulting in a total of $pb = b^d$ new bonds. Repeated iteration of this procedure for each new bond generates an infinite pseudo-lattice, which might be called a "Berker lattice"; it has a hierarchical structure characterized by the two independent parameters b and p. In principle both b and p should be integral but, as will be seen, the recursion relations extend naturally to general values so corresponding to a continuous effective dimensionality $d = 1 + \ln_b p$.[20]

The *zeroth level* of the hierarchy, I_0, comprises all lattice sites of coordination number $q_0 = 2$. At the next or first level, I_1, the coordination number of the sites is $q_1 = 2p$. The nth level, I_n, contains all sites of coordination number $q_n = 2p^n$. The number of sites in I_n, per bond of the infinite structure, is $(b-1)/b^{n+1}p^n$. It is because the infinite lattice contains (for $p > 1$) infinite sets of sites of unbounded coordination number that true phase transitions can occur at positive temperature in contrast to the similar "truncated tetrahedron lattice" introduced by Nelson and Fisher.[23]

Now at each site i let there be a "spin" variable s_i which might be a simple Ising spin, as in our explicit calculations, but which may equally well be any discrete or continuous type of variable. Let $j_\mu(s)$, for $\mu = 1, 2, \ldots$, represent various single-site or field terms and $k_\nu(s,s')$, for $\nu = 1, 2, \ldots$, represent coupling terms between nearest-neighbor spins. In our case we have $j_1(s) = s$, $j_2(s) = s^2$, and $k_1(s,s') = ss'$, $k_2 = s^2 s'^2$, and $k_3 = \frac{1}{2}(s^2 s' + ss'^2)$. Then we consider the general class of Hamiltonians given by

$$-\frac{\mathcal{H}}{k_B T} = \sum_\mu \sum_{n=0} \sum_{i \subset I_n} H_{\mu,n} j_\mu(s_i) + \sum_\nu \sum_{\langle ij \rangle} K_\nu k_\nu(s_i, s_j) \quad . \tag{A1}$$

In order to carry the information about the renormalization of the free energy is also useful to include a "constant" term, $k_0 \equiv 1$. Note particularly, that we allow for fields, $H_{\mu,n}$, of different strengths on different levels of the hierarchy, even though we suppose all bonds represent identical couplings, K_ν, independent of the levels of the hierarchy to which the terminal sites belong. (Clearly, at the cost of even further loss of the restricted translational invariance, one could generalize to allow for $K_{\nu,n,n'}$ couplings.)

Now define the renormalized fields and interactions obtained by the decimation or dedecoration of a linear chain (the case $p = 1$) by a scale factor b as[23]

$$K_\nu^\nabla \equiv K_\nu^\nabla(\{H_{\mu,0}\}, \{K_{\nu'}\}) \quad , \tag{A2}$$

$$H_{\mu,0}^\nabla \equiv H_\mu^\nabla(\{H_{\mu',0}\}, \{K_\nu\}) \quad . \tag{A3}$$

Note that $H_{\mu,0}^\nabla$ and K_ν^∇ can be computed in terms of the bth power of the appropriate transfer matrix or integral operator. If the eigenvalues of this operator are $\Lambda_r(\{H_{\mu,0}\}, \{K_\nu\})$, $r = 0, 1, 2, \ldots$, the transformation can clearly be expressed as a weighted sum on $r \geq 0$ of the powers $(\Lambda_r)^b$. This clearly provides a natural extension to arbitrary b.

The exact general recursion relations of the Migdal-Kadanoff type renormalization group for arbi-

trary b and p can now be written compactly as

$$K_\nu' = pK^\nabla(\{H_{\mu,0}\}, \{K_{\nu'}\}) \ , \tag{A4}$$

$$H'_{\mu,n} = p^{n+1}[H^\nabla_{\mu,0}(\{H_{\mu',0}\}, \{K_\nu\}) - H_{\mu,0}] + H_{\mu,n+1} \ , \tag{A5}$$

for $n = 0, 1, 2, \ldots$. The second relation follows by considering the association of the single-site terms with the bonds at each level of the hierarchy and noting that sites of level $n+1$ become the new sites at level n. Thus a field $H_{\mu,0}$, provided equally by the sites at each end of every bond, is associated with each bond, while a field $H_{\mu,n} - p^n H_{\mu,0}$ remains on each site in I_n during the dedecoration process.

Now we are at liberty, in selecting models, to choose the values $H_{\mu,n}$ at the nth level of the hierarchy in any convenient fashion! To this end it is natural to set

$$H_{\mu,n} = f_{\mu,n} H_\mu \text{ with } H_\mu \equiv H_{\mu,0} \ , \tag{A6}$$

where, as the thermodynamic conditions, i.e., the fields, and couplings, H_μ and $K_{\nu'}$ are varied the factors $f_{\mu,n}$ remain fixed. Indeed it is easy to verify that the "standard assignment"

$$f_{\mu,n} = f^0_{\mu,n} \equiv p^n \ , \tag{A7}$$

is, for any given μ, preserved under the renormalization-group recursion relation (A5). This assignment is the one that corresponds to the usual implementation of the Migdal-Kadanoff-type schemes which we have used for the fields D and H throughout this paper.[10] Evidently the fields at the nth level then increase exponentially in direct proportion to the coordination number q_n.

In general, any assignment differing from (A7) will not remain invariant under renormalization. However, if for some $\mu = \bar{\mu}$, with $H_{\bar{\mu},0} \equiv \bar{H}$, the special condition

$$\bar{H}^\nabla \equiv \bar{H}^\nabla(\{H_{\mu,0}\}, \{K_\nu\}) = r\bar{H} \tag{A8}$$

is satisfied, another invariant choice is possible. This condition, in which the factor r is supposed fixed, independent of all the $H_{\mu,0}$ and K_ν, is motivated by what happens when a dilution field is introduced in the spin-1 Ising model we have been addressing. It is then found that (A8) holds generally with $r = 1$. The origin of this simple result is that dilution, by removal of a spin at a site i on a one-dimensional chain, yields essentially the identical decoupling of the terminal spins as does the occurrence, already allowed for, that the spin i is in the state with $s_i = 0$. Thus the only effect of the dilution field is to reweight the zero spin state relative to the $s_i = \pm 1$ states. Indeed on a standard, uniform space lattice the Hamiltonian (4.1) with dilution maps onto the original, undiluted Hamiltonian (1.1) with transformed interactions $(\tilde{J},\tilde{K},\tilde{D},\tilde{H},\tilde{H}_3) = (J,K,D+D_0,H,H_3)$ where $D_0 = \frac{1}{2} q \ln(1+z)$.

In any event it is not hard to check for the hierarchical lattices that when (A8) holds the special assignment

$$f_{\bar{\mu},n} = \bar{f}_n = \frac{r(p-\bar{p})(r\bar{p})^n + (1-r)p^{n+1}}{p - r\bar{p}} \ , \tag{A9}$$

where $\bar{p}$ is arbitrary, is invariant under the recursion relation (A5) which then reduces to

$$H'_{\mu,n} = \bar{f}_n \bar{p} H^\nabla_{\bar{\mu},0} = \bar{f}_n r\bar{p} H_{\bar{\mu},0} \ , \tag{A10}$$

or equivalently, simply to

$$\bar{H}' = r\bar{p}\bar{H} \ . \tag{A11}$$

Evidently if one chooses $\bar{p}$ so that $r\bar{p} = 1$, the special field $\bar{H}$ becomes a renormalization-group invariant (corresponding to a fixed marginal operator). For our spin-1 model with $r = 1$ for dilution, it thus suffices to take $\bar{p} = 1$ to obtain an invariant dilution field. This then corresponds to the rather natural assignment $\bar{f}_n = 1$ (all n) corresponding to choosing the *same* dilution field, $\bar{H} \equiv P$, at all sites whatever their level in the hierarchy! For the other fields in the model, namely, H and D, for which the one-dimensional recursion relations do not have the special form (A8), we retain the standard assignment (A6).

It is appropriate finally to record explicitly the recursion relations for the dilute system which we actually utilize. It is convenient to introduce the notation

$$u = \exp[-(J+K-D-H)/q] \ , \tag{A12}$$

$$v = \exp[-(J+K-D+H)/q] \ , \tag{A13}$$

$$w = \exp[(2H+H_3)/q] \ , \tag{A14}$$

$$x = \exp[-(J+K-2D)/q] \ , \tag{A15}$$

$$y = \exp(-2J/q), \quad z = \exp(2P/q) \ . \tag{A16}$$

Then the recursion relations become $z' = z$, reflecting the invariance of the dilution field, and, recalling that $p = b^{d-1}$,

$$u' = \frac{[wu + xu(1+z) + yv]^p}{[w^2 + y^2 + u^2(1+z)]^{p/2}[w^{-2} + y^2 + v^2(1+z)]^{p/2}} \ , \tag{A17}$$

$$v' = \frac{[uy + vx(1+z) + vw^{-1}]^p}{[w^2 + y^2 + u^2(1+z)]^{p/2}[w^{-2} + y^2 + v^2(1+z)]^{p/2}} \ , \tag{A18}$$

$$w' = \left[\frac{w^2 + y^2 + u^2(1+z)}{w^{-2} + y^2 + v^2(1+z)}\right]^{p/2} \ , \tag{A19}$$

$$x' = \frac{[u^2 + x^2(1+z) + v^2]^p}{[w^2 + y^2 + u^2(1+z)]^{p/2}[w^{-2} + y^2 + v^2(1+z)]^{p/2}} \ , \tag{A20}$$

$$y' = \frac{[wy + w^{-1}y + uv(1+z)]^p}{[w^2 + y^2 + u^2(1+z)]^{p/2}[w^{-2} + y^2 + v^2(1+z)]^{p/2}} \ . \tag{A21}$$

There is also an independent relation, which we do

not quote, for the "constant term" in the Hamiltonian which is needed to determine the free energy, etc.

It is worth remarking that if the dilution field had been introduced with the standard assignment (A7) its recursion relation would have been $z' = z^p$ while (A17) to (A21) would not change. Fixed points would then be: (a) $z^* = 0$ which clearly yields the original, undiluted results; (b) $z^* = 1$, which is unstable but has the new exponents reported for $z = 1$ in the invariant case; and (c) $z^* = \infty$, which, by a change of variables as $z \to \infty$, can be shown to yield essentially the same results as $z = 0$.

[1]M. Kaufman, R. B. Griffiths, J. M. Yeomans, and M. E. Fisher, Phys. Rev. B 23, 3448 (1981); this paper will be denoted I.

[2]A. A. Migdal, Sov. Phys. JETP 42, 743 (1976); L. P. Kadanoff, Ann. Phys. (N.Y.) 100, 359 (1976).

[3]S. Sarbach and M. E. Fisher, Phys. Rev. B 18, 2350 (1978); R. B. Griffiths, *ibid.* 12, 345 (1975).

[4]M. J. Stephen, Phys. Lett. 56A, 149 (1976), has reported the result to leading order in $\epsilon = d - 1$ for the Potts point, but other exponents and the full fixed point structure predicted for $d = 1 + \epsilon$ have not been presented previously.

[5]S. Krinsky and D. Furman, Phys. Rev. Lett. 32, 731 (1974); Phys. Rev. B 11, 2602 (1975).

[6]This is inspired by the work of B. Nienhuis, A. N. Berker, E. K. Riedel, and M. Schick, Phys. Rev. Lett. 43, 737 (1979).

[7]R. B. Griffiths, J. Chem. Phys. 60, 195 (1974).

[8]J. C. Lang and B. Widom, Physica 81A, 190 (1975).

[9](a) M. E. Fisher and S. Sarbach, Phys. Rev. Lett. 41, 1127 (1978); (b) S. Sarbach and M. E. Fisher, Phys. Rev. B 20, 2797 (1979).

[10]J. V. José, L. P. Kadanoff, S. Kirkpatrick, and D. R. Nelson, Phys. Rev. B 16, 1217 (1977), Appendix B.

[11]A. N. Berker and S. Ostlund, J. Phys. C 12, 4961 (1979); G. Forgács and A. Zawadowski, Report No. KFKI-1977-103, Central Research Institute for Physics, Budapest (unpublished).

[12]D. Furman, S. Dattagupta, and R. B. Griffiths, Phys. Rev. B 15, 441 (1977); see the bibliography in this paper for references to earlier work on classical and mean-field theory.

[13]E. K. Riedel and F. J. Wegner, Phys. Rev. Lett. 29, 349 (1972); Phys. Rev. B 7, 248 (1973).

[14]M. J. Stephen, E. Abrahams, and J. P. Straley, Phys. Rev. B 12, 256 (1975); M. J. Stephen, *ibid.* 12, 1015 (1975).

[15]M. E. Fisher, in *Magnetism and Magnetic Materials—1974,* edited by C. D. Graham, G. H. Lander, and J. J. Rhyne, AIP Conf. Proc. No. 24 (AIP, New York, 1975), p. 273.

[16]M. J. Stephen and J. L. McCauley, Phys. Lett. A 44, 89 (1973); T. S. Chang, G. F. Tuthill, and H. E. Stanley, Phys. Rev. B 9, 4882 (1974); G. F. Tuthill, J. F. Nicoll, and H. E. Stanley, *ibid.* 11, 4579 (1975); F. J. Wegner, Phys. Lett. A 54, 1 (1975).

[17]M. P. M. den Nijs, J. Phys. A 12, 1857 (1979); B. Nienhuis, E. K. Riedel, and M. Schick, *ibid.* 13, L189 (1980).

[18]A. N. Berker and M. Wortis, Phys. Rev. B 14, 4946 (1976).

[19]T. W. Burkhardt, Phys. Rev. B 14, 1196 (1976); T. W. Burkhardt and H. J. F. Knops, *ibid.* 15, 1602 (1977).

[20]Y. Gefen, B. B. Mandelbrot, and A. Aharony, Phys. Rev. Lett. 45, 855 (1980).

[21]B. Nienhuis and M. Nauenberg, Phys. Rev. B 13, 2021 (1976).

[22]D. P. Landau and R. H. Swendson, Phys. Rev. Lett. 46, 1437 (1981).

[23]D. R. Nelson and M. E. Fisher, Ann. Phys. (N.Y.) 91, 226 (1975).